Advances in Military Technology
Vol. 21, No. 1, 2026, pp. 177-194
ISSN 1802-2308, eISSN 2533-4123
DOI 10.3849/aimt.02079

Evaluation of Wheeled Robot Mobility Limits on Unstructured Terrain

P. Huy Dang[1*], and M. Nowakowski[2]

[1] *Faculty of Military Technology, University of Defence, Brno, Czech Republic*
[2] *Military Institute of Armoured and Automotive Technology, Sulejówek, Poland*

The manuscript was received on 11 January 2026 and was accepted after revision for publication as an original research paper on 3 April 2026.

Abstract:

This paper examines the mobility limits of a wheeled mobile robot on unstructured and deformable terrain, where surface variations affect traction and navigation. A digital twin of the robot was developed in ROS 2 and Gazebo Classic using real geometry, drive parameters, and sensor specifications. Simulations on cohesive mud, loose sand, and inclined surfaces analyzed wheel-terrain interaction. Robot motion was assessed via wheel odometry, IMU, and GNSS to measure slip and velocity errors. Results were validated with field tests on sandy terrain, showing consistent trends in traction loss, slip, and sensor degradation. Findings emphasize terrain impact on mobility and the need for terrain-aware, multi-sensor evaluation frameworks.

Keywords:

wheeled mobile robot, deformable terrain, mobility limitation, digital twin, IMU/GNSS fusion, terrain-adaptive navigation, Gazebo simulation

1 Introduction

Autonomous ground robots are increasingly expected to operate in unstructured outdoor environments where terrain complexity imposes strict limits on mobility, safety, and mission success [1]. The ability of a wheeled mobile robot to traverse non-engineered surfaces, including loose soils, gravel, uneven, rocky ground, and steep slopes, is a critical determinant of operational autonomy across applications such as precision agriculture, infrastructure inspection, search and rescue, and military reconnaissance [2].

Terrain traversability, defined as the capacity of the mobile robot to progress through the environment while maintaining control, localization, and mission con-

* *Corresponding author: Department of Military Robotics, Faculty of Military Technology, University of Defence, Kounicova 156/65, CZ-662 10 Brno, Czech Republic. Phone: +420 732 86 21 15, E-mail: huydang.pham@unob.cz. ORCID 0009-0007-4895-6430.*

straints, represents a fundamental concept in mobile robotics [3]. Traversability assessment combines perception to sense surface geometry and properties, vehicle modelling to predict wheel-terrain interaction, and path planning to select feasible and safe routes [4, 5]. Accurate metrics are essential for both reactive control and long-term planning because estimation errors, due to slip or sinkage, directly lead to mission failures or loss of mobility.

Developing robust traversability estimators and mobility controllers for wheeled robots presents multiple challenges. It should be highlighted that geomorphic variability (grain size, cohesion, roughness) produces heterogeneous contact mechanics that are difficult to observe directly and often require indirect estimation from proprioceptive and exteroceptive sensors [6]. On the other hand, wheel slip and wheel sinkage are non-linear functions of vehicle load, wheel geometry, motor torque, and soil shear strength; substantial slip may occur suddenly on transitions, causing odometry errors and control failures [7–9]. Additionally, slopes and obstacles change normal loads and wheel-ground normal angles, compounding traction loss and increasing energy consumption. Field observations and experimental studies, including multi-agent maneuver models, have been used to validate theoretical mobility predictions and assess cooperative ground operations [10, 11]. Furthermore, GNSS signal degradation in forested or complex terrain can significantly affect localization accuracy for off-road vehicles, highlighting the need to incorporate environmental effects into traversability and navigation models [12].

Field testing of wheeled platforms across a wide range of terrains is costly, time-consuming, and sometimes unsafe; consequently, high-fidelity simulation and digital twin approaches have become central to pre-deployment evaluation and algorithm development. Available environments that model contact dynamics and realistic sensor simulation enable systematic studies of wheel-terrain interaction and sensor fusion strategies under controlled, repeatable conditions [13]. Simulation has been successfully used to train traversability classifiers to evaluate energy models and to validate slip-compensation algorithms before field trials [14].

Despite these advances, a gap remains between simulated and field behavior: many traversability models primarily consider terrain geometry while under-representing robot-specific parameters such as motor torque limits, encoder resolution and noise, and detailed IMU/GNSS characteristics that influence navigation performance in real deployments. The gap between simulation and real-world performance can be addressed by parameterizing digital twins with experimentally measured sensor and actuator characteristics [15, 16]. Incorporating manufacturer specifications, such as motor torque, IMU noise density, and RTK GNSS accuracy, improves the realism of the virtual experiments and makes the simulation results more interpretable for hardware design and control tuning.

Recent literature has identified several complementary directions for improving traversability evaluation and mobility prediction, including the development of physics-aware traversability metrics that consider wheel–soil interaction and slip dynamics, sensor-fusion methods that combine encoders, IMU, and vision or GNSS to detect and compensate for slip and drift, and experimental frameworks, either simulated or field-based, that systematically vary terrain parameters, slopes, and payloads to characterize mobile robot behavior across operational conditions [17, 18]. Energy efficiency is an additional operational constraint that strongly couples with traversability: energy per meter increases with slope and payload and grows disproportionately when slip occurs, because wasted motor work does not produce forward progress. Hence, energy models that combine motor limits, drivetrain efficiency, and terrain resistance are necessary for realistic mission planning, and several recent studies have proposed empirical and model-based methods to estimate energy consumption for all-terrain robots [19].

This study was motivated by the need to establish a reproducible, high-fidelity evaluation framework that integrates a digital twin of a wheeled mobile robot parameterized with actual actuator and sensor specifications, physics-based terrain models with variable friction and slope implemented in Gazebo, and an automated batch execution pipeline that systematically modifies terrain friction, slope, and payload while recording synchronized sensor data for subsequent analysis. Through the combination of simulation and sensor-level realism, the objective was to quantify mobility limitations, including slip ratio, odometry drift, GNSS-calculated speed, IMU-derived speed, and signal noise, across representative operational scenarios, and to generate reproducible visualizations suitable for method comparison and design optimization [1, 20, 21].

In addition, selected simulation scenarios were experimentally validated using real-world data collected from the same mobile robot during testing on sandy terrain. The proposed methodology extends prior work on traversability modelling, slip estimation, and digital twin validation by explicitly varying robot-level parameters and using manufacturer-rated actuator and sensor properties to produce realistic, interpretable simulation results. Experimental insights from cooperative maneuver studies [10], LiDAR-based vegetation and terrain analysis [11], and GNSS signal quality assessments in forested environments [12] further support the need to integrate environment-specific factors in mobility prediction and digital twin parameterization.

2 Robot Platform Description

A wheeled robotic platform developed by [22] referred to as Elevate, was used in a customized configuration equipped with additional sensors described in this section (Fig. 1). The experimental platform study is a medium-sized mobile robot designed to support special-purpose missions in unstructured environments, where mobility, adaptability, and cost-efficiency are essential. The robot was developed as a budget-oriented solution, optimized to balance operational performance with affordability. This design philosophy led to the use of a stereo vision system with depth-sensing capability instead of a more expensive LiDAR unit, providing sufficient terrain perception and obstacle detection while maintaining cost-effectiveness.

Fig. 1 Wheeled robotic platform used in this study

The platform is powered by four electric motors, each equipped with a planetary gearbox and a wheel encoder. This drivetrain provided sufficient torque to manage off-road mobility while maintaining satisfactory energy efficiency for reconnaissance and support tasks. The platform's dimensions and mass characteristics, as shown in Tab. 1, allowed operation in confined or cluttered environments such as forests, rubble fields, or industrial facilities.

Tab. 1 Main physical and mechanical parameters of the robotic platform

Parameter	Value	Unit
Total mass	32	kg
Payload capacity	60	kg
Drive type	Differential drive	–
Number of motors	4 × 150 W	–
Maximum motor speed	~11 700	rev/min
Maximum motor torque	200	mN·m
Maximum linear velocity	2	m/s
Chassis dimensions (L × W × H)	0.678 × 0.655 × 0.250	m
Wheel diameter	0.350	m
Wheel width	0.145	m
Ground clearance	0.140	m
Wheelbase	0.420	m

The onboard sensor set was intentionally simplified to balance robustness and affordability. The primary exteroceptive sensors included a stereo camera and a standard IP camera, providing both RGB and depth data for terrain reconstruction and obstacle detection. The proprioceptive sensors consisted of an inertial measurement unit (IMU) and wheel encoders used for odometry estimation. For outdoor localization, the system incorporated a global navigation satellite system (GNSS) receiver. Together, these sensors enabled the collection of data required for localization, perception, and mobility analysis under various terrain conditions, as shown in Tab. 2.

Tab. 2 Main installed sensors

Sensor type	Model	Key specifications	Function
Inertial/GNSS unit	MTi-680G RTK GNSS/INS	Update rate: up to 400 Hz; Orientation accuracy: <0.2°; Position accuracy: ±1.5 m (RTK < 0.02 m)	Orientation, navigation, and absolute positioning
Stereo camera	ZED 2	FOV: 110° × 70°; Resolution: 4 416 × 1 242 @ 15 FPS; Depth range: 0.2–20 m	Terrain perception, obstacle detection, and 3D reconstruction
Wheel encoders	HEDS 5 540	500 counts per turn (3 channels)	Odometry and wheel velocity estimation

The platform used represents a mission-driven compromise between performance and cost. It provides adequate payload capacity, stability, and terrain adaptability while minimizing financial overhead by replacing expensive sensor modalities with a depth-capable stereo vision system. This configuration enables systematic investigation of mobility constraints and localization accuracy in unstructured terrain. It remains representative of deployable, cost-efficient robotic systems designed for operation in hazardous or resource-limited environments.

3 Simulation Environment

In this study, the platform described in Section 2 was modeled in ROS 2 and Gazebo to support both experimental and simulation tasks, thereby providing a controlled framework for analyzing the dynamic behavior and sensor response of a wheeled mobile robot traversing deformable terrain with varying densities and inclinations. The simulated platform represented an off-road mobile robot with a differential-drive configuration and a four-wheel chassis geometry, reflecting the proportions and kinematics of the used unit. The robot model was defined in URDF/Xacro format, ensuring structural consistency and realistic mass and inertia distribution for all mechanical components, including chassis, wheels, and sensor frames (Fig. 2).

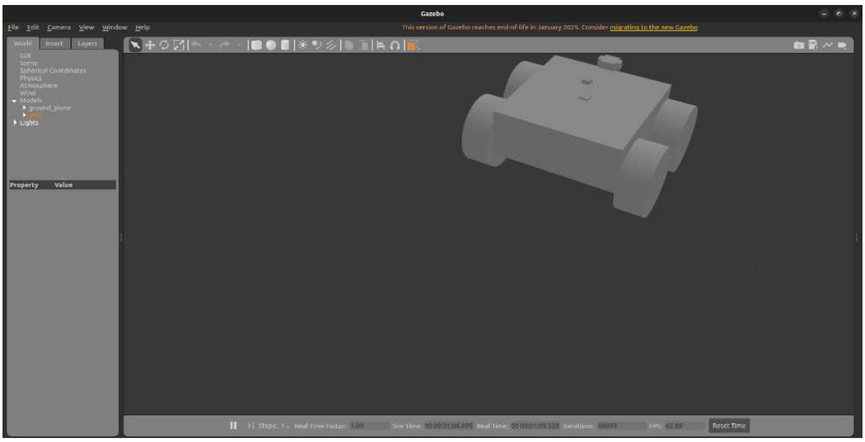

Fig. 2 Robot model in Gazebo simulation environment

The simulation accounted for wheel-terrain interaction using the Gazebo Classic physics engine with the ODE solver. Two sand surface configurations loose and medium-density sand were defined to represent terrains with different compaction levels and load-bearing capacity. Additionally, a cohesive, high-viscosity mud configuration was introduced to model a deformable surface inducing significant wheel slip and delayed motion initiation. Wheel–terrain interaction was modeled using the ODE contact formulation, with effective friction parameters specified in the Gazebo world description file. For each terrain type, Coulomb friction coefficients μ_1 and μ_2 and viscous contact damping terms were assigned. These parameters represent effective contact properties within the physics engine rather than laboratory-measured Coulomb friction coefficients of soil samples.

Distinct values of μ_1 and μ_2 were used for medium–density sand, loose sand, and cohesive mud to emulate differences in traction, shear resistance, and energy dissipation observed in real off-road conditions, see Tab. 3. The parameter values were selected based on ranges reported in robotics and vehicle-terrain interaction literature and subsequently refined through iterative calibration to reproduce qualitatively realistic mobility phenomena, including delayed acceleration, increasing wheel slip with speed, and complete immobilization on cohesive mud after exceeding a critical slip threshold.

Tab. 3 Effective wheel-terrain friction parameters used in Gazebo-ODE simulation

Terrain type	**μ_1 (ODE)**	**μ_2 (ODE)**	**Interpretation / effect**
Medium-density sand	0.8–1.0	0.8–1.0	Stable traction, limited slip
Loose sand	0.4–0.6	0.4–0.6	Increased slip, reduced acceleration
Cohesive mud	0.1–0.2	0.1–0.2	Rapid loss of mobility, immobilization

Applied coefficients should be interpreted as effective friction parameters implicitly capturing combined effects of rolling resistance, sinkage, shear deformation, and viscous soil behavior within the ODE contact model, rather than as physical soil friction constants.

The slope variant, corresponding to a 5° inclined plane (Fig. 3), was introduced for the sand cases to replicate gravity-induced traction loss and asymmetric wheel loading.

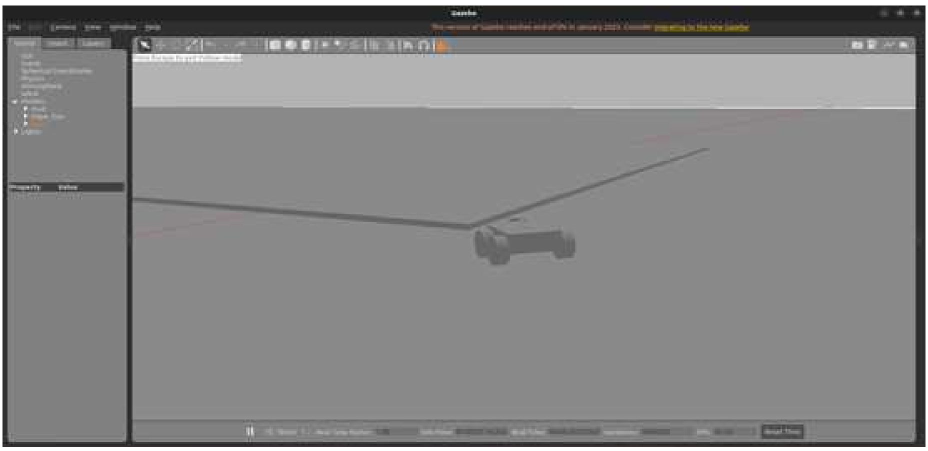

Fig. 3 Inclined-plane scenario (5° slope) in simulation environment

The robot was equipped with a virtual multi-sensor, including:

- wheel odometry providing linear and angular displacement,
- inertial Measurement Unit (IMU) streaming angular velocities and linear accelerations,
- GNSS receiver producing position fixes and velocity readings,
- ground truth source derived from Gazebo’s model, providing reference pose and velocity data for comparison.

The mobile robot was actuated with a sinusoidal velocity command profile given by the following relation.

$$v(t) = 1.0 + 0.5 \sin \frac{2\pi t}{60} \tag{1}$$

Each cycle was set to 300 seconds of driving. Defined excitation forced the robot to accelerate and decelerate periodically between approximately 0.5 m/s and 1.5 m/s, with additional short stop phases inserted to evaluate stationary slip and recovery. This profile was intentionally designed to excite both transient and steady-state traction regimes and to simulate realistic maneuvering conditions observed in low-speed off-road driving. Each simulation run generated a ROS 2 bag file containing synchronized sensor, control, and ground-truth data streams.

Post-processing of the recorded experiments was performed using Python tools within the ROS 2 environment. Each ROS bag was parsed into time-synchronized arrays representing odometry, IMU, GNSS, and ground-truth data. All-time series were aligned using asynchronous time matching with a 50 m/s tolerance to ensure temporal consistency between sensors. Zero-mean Gaussian noise was applied to the GNSS signals to emulate realistic outdoor measurement noise (e.g., multipath). Odometry and IMU sensors remained deterministic but were physically affected by wheel slip, uneven traction, and terrain deformation, ensuring that observed deviations originated from simulated physics rather than artificial measurement corruption.

The relationship among commanded, odometry, and ground-truth velocities was visualized to highlight the deviations introduced by surface deformation and traction loss.

Fig. 4 shows that during the first 60 s, the robot followed the sinusoidal command trajectory with moderate adherence. However, after this period, the vehicle became immobilized due to excessive sinkage and loss of traction, as indicated by near-zero odometry and ground-truth velocities. This behavior is characteristic of cohesive mud, where high viscosity and suction forces prevent wheel recovery once slip exceeds the critical threshold. The flattening of the odometry curve confirms total immobilization caused by a buildup of soil resistance.

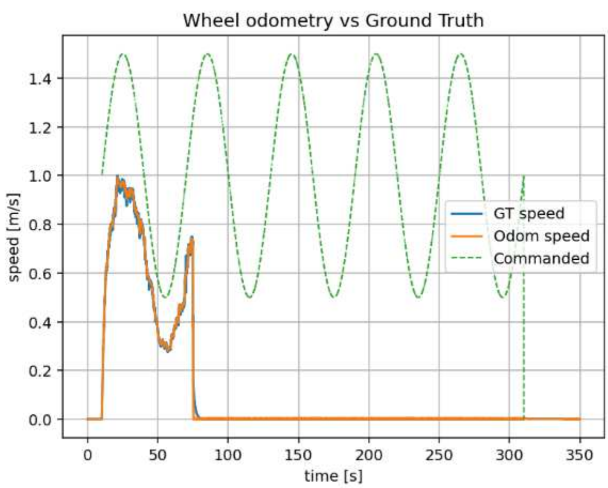

Fig. 4 Wheel odometry versus ground-truth velocity on mud terrain

In contrast, Fig. 5 presents the corresponding results for loose and medium-density sand, respectively. On loose sand, partial slippage occurred during the acceleration phases, as evidenced by a lag between the commanded and realized velocities. Nevertheless, the robot maintained continuous motion throughout the trajectory. The medium-density sand case produced the most stable response, with a near-linear correlation between commanded and measured speeds, indicating adequate traction and minimal wheel deformation.

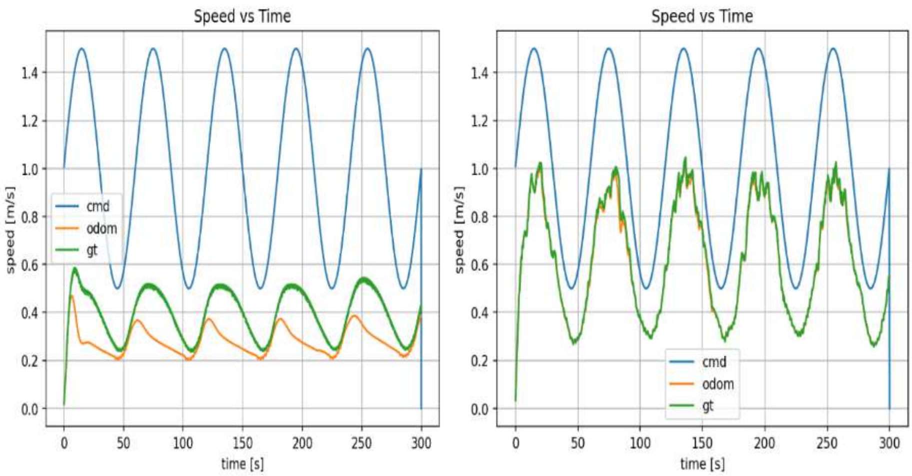

Fig. 5 Wheel odometry versus ground-truth velocity for loose (left) sand and medium-density sand (right)

Additionally, a slip proxy was computed using the following relation:

$$s(t) = 1 - \frac{v_{\text{odom}}(t)}{v_{\text{gt}}(t)} \tag{2}$$

Here, $v_{\text{odom}}(t)$ denotes the forward speed estimated from wheel odometry (encoder-based), and $v_{\text{gt}}(t)$ denotes the ground-truth forward speed provided by the simulator. Values of $s(t)$ close to zero indicate good agreement. In contrast, large magnitudes $|s(t)|$ indicate strong decoupling between wheel rotation and vehicle motion (severe slip) or near-zero ground-truth motion. Because the definition uses $v_{\text{gt}}(t)$ in the denominator, the metric becomes ill-conditioned when $|v_{\text{gt}}(t)|$ approaches zero; therefore, mean values were computed only over samples where $|v_{\text{gt}}(t)|$ exceeded a small threshold.

On mud, the slip proxy in Fig. 6 shows a rapid growth in $|s(t)|$ after the onset of sinkage, confirming that wheel rotation no longer translates into forward motion. The subsequent fluctuations are consistent with intermittent wheel spin and stick-slip behavior, in which input energy is dissipated through terrain deformation rather than being converted into traction.

IMU analysis focused on the yaw-rate component (ω_z), capturing rotational disturbances associated with lateral instability and traction irregularities. Fig. 7 shows the time evolution of ω_z for the mud terrain. High-frequency fluctuations during the first ≈60 s correspond to steering corrections during the initial motion phase, followed by a drop to near zero once the vehicle becomes immobilized.

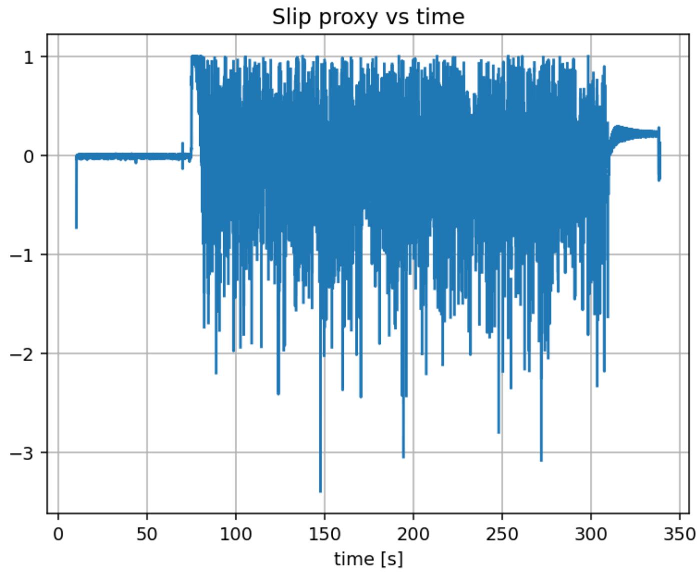

Fig. 6 Slip proxies (t) over time for mud terrain

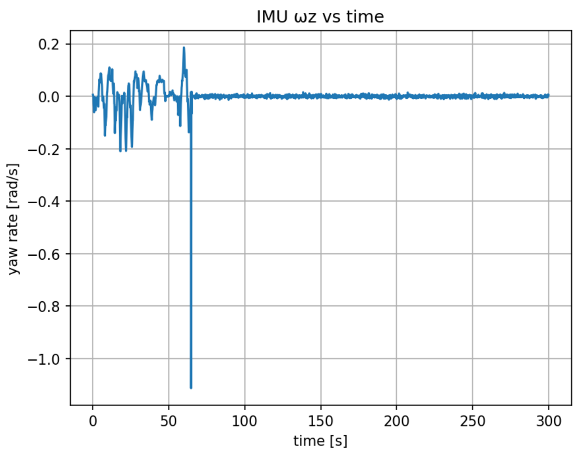

Fig. 7 IMU yaw rate ω_z over time for mud terrain

For loose and medium-density sand (Fig. 8), the IMU yaw-rate signal remains active throughout the simulation, indicating sustained rotational dynamics and reduced vibrational noise compared with mud. The medium-density sand exhibits smoother oscillations, suggesting a more consistent transfer of wheel torque into forward motion.

The GNSS-derived speed plots (Fig. 9) were analyzed as a proxy for signal stability and noise behavior under varying terrain and motion conditions. In the sand case (Fig. 9b), the GNSS speed exhibits sinusoidal motion with mild disturbances due to local changes in acceleration. Occasional peaks are simulated signal noise rather than physical anomalies, thereby replicating realistic GNSS performance under uneven, semi-structured outdoor conditions.

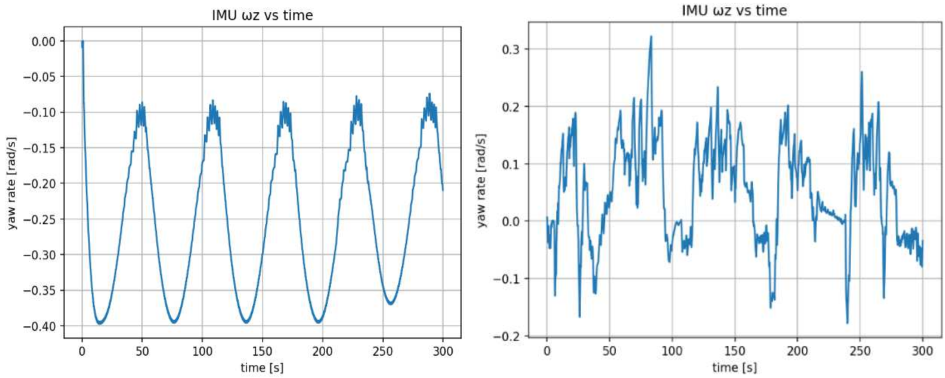

a) *b)*

Fig. 8 IMU yaw rate ω_z over time for a) loose sand and b) medium-density san

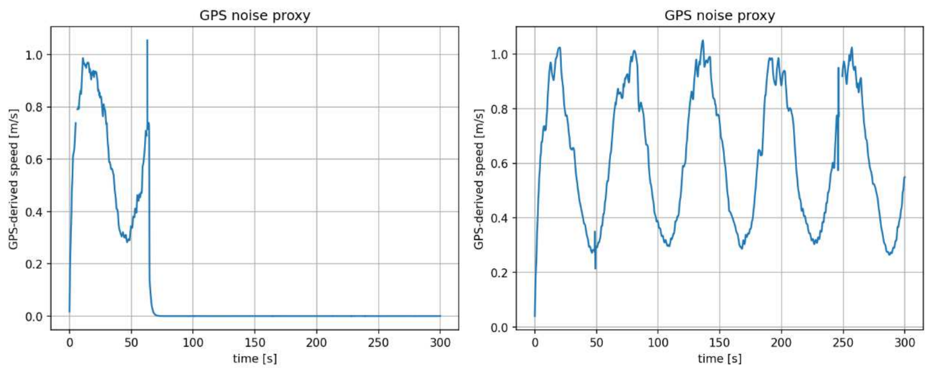

a) *b)*

Fig. 9 GNSS-derived speed over time for a) mud and b) sand terrain

Gazebo provided ground-truth pose and velocity data, serving as a precise reference for linear velocity and displacement. To suppress transient numerical fluctuations, a low-pass filter was applied to all velocity profiles. GNSS-based velocities were obtained from finite differences of ENU coordinates and subsequently smoothed to assess signal noise and jitter. This post-processing procedure enabled quantitative characterization of kinematic behavior and sensor performance under different terrain resistances and inclinations. The combined evaluation of odometry, IMU, and GNSS data offers insight into nonlinear wheel-terrain interaction and sensor degradation arising from slip, vibration, and rolling resistance.

The mean slip proxy magnitude and sensor speed errors (see Tab. 4) show a clear dependence on terrain deformability. On cohesive mud, odometry and IMU errors remained low during the moving phase, while the GNSS speed error increased (45.7 %), indicating reduced precision during slow or irregular motion. On loose sand (5° slope), the slip proxy and odometry error increased (≈27 %), confirming the impact of reduced friction and slope-induced sliding; IMU and GNSS errors were lower

(9.3 % and 17.9 %), suggesting improved signal stability at moderate speeds. The medium-density sand case yielded the most stable wheel-ground coupling (|s|≈1 %) and the lowest odometry error (1.4 %). Yet, the GNSS error rose to 57.1 %, likely due to oscillatory motion and intermittent stops that amplify relative GNSS velocity uncertainty.

Tab. 4 Comparative analysis of slip and sensor velocity errors across terrains

Terrain	**Mean $\|s(t)\|$ [%]**	**Mean odometry error [%]**	**Mean IMU error [%]**	**Mean GNSS error [%]**
Cohesive mud (flat)	2.0	2.6	4.9	45.7
Loose sand (5° slope)	27.0	27.0	9.3	17.9
Medium-density sand (5° slope)	1.0	1.4	7.3	57.1

Overall, the results show that terrain deformability and traction variability strongly affect sensor performance. Odometry is most sensitive to slip, IMU signals capture short-term dynamics but may drift when integrated over time, and GNSS measurements tend to degrade during slow or irregular motion. These observations underscore the need for adaptive, terrain-aware sensor fusion that adjusts data weighting based on detected surface conditions.

4 Results and Discussion

The mobility performance of the wheeled mobile robot was evaluated on unstructured sandy terrain characterized by variable compaction and irregular surface geometry.

The testing area (see Fig. 10) consisted of loose and semi-compacted sand typical of off-road and forest environments. Such conditions resulted in uneven traction, wheel sinkage, and slip, which significantly affected the robot's locomotion efficiency and steering stability.

Fig. 10 Field test of the wheeled mobile robot on sandy terrain

The sandy surface produced distinct high-frequency vibrations, as evidenced by the recorded IMU signals (see Fig. 11), corresponding to short, high-amplitude acceleration peaks during the robot's traversal.

DOI 10.3849/aimt.02079

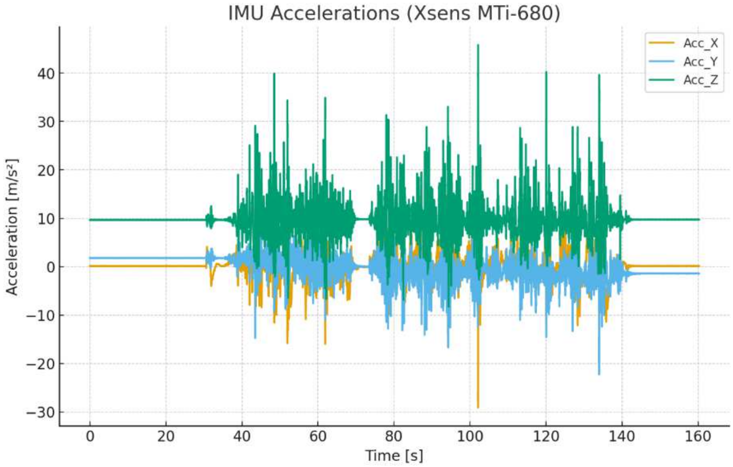

Fig. 11 IMU acceleration signals recorded during sandy-terrain traversal

The experimental platform used an Xsens MTi-680 inertial navigation unit that combines a triaxial accelerometer, gyroscope, barometer, and integrated GNSS receiver. The sensor was mounted near the robot's center of gravity to minimize rotational artifacts. During the test, the MTi-680 recorded a complete motion dataset at 100 Hz, including linear acceleration, angular velocity, orientation, altitude, and GNSS-based position and velocity.

The GNSS measurements in Fig. 12 show the robot's motion along a short outdoor path. The latitude-longitude trace (Fig. 12a) exhibits minor, consistent variations, confirming that the GNSS maintained reliable satellite visibility with only minor positional noise due to partial forest canopy and multipath reflections.

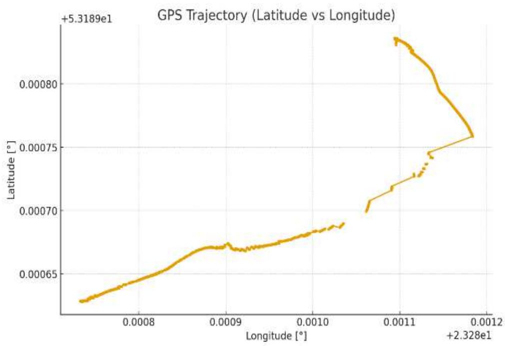

a)

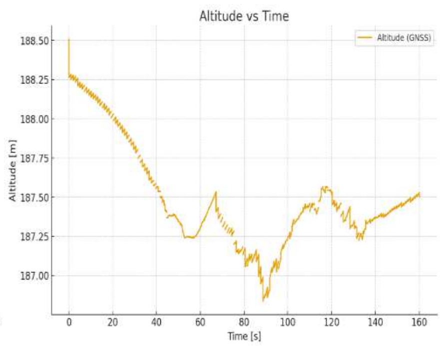

b)

Fig. 12 GNSS measurements: (a) latitude–longitude trajectory and (b) altitude over time

The altitude evolution over time shows oscillations within approximately ±1 m, attributed primarily to GNSS accuracy limits rather than actual terrain undulation (Fig. 12b). These variations illustrate the influence of environmental conditions and local reflectivity on GNSS precision when operating in natural terrain.

The ENU velocity components reported by the GNSS/INS unit v_E and v_N (Fig. 13) were used to compute the horizontal ground speed:

$$v_{\text{ground}} = \sqrt{v_E^2 + v_N^2} \tag{3}$$

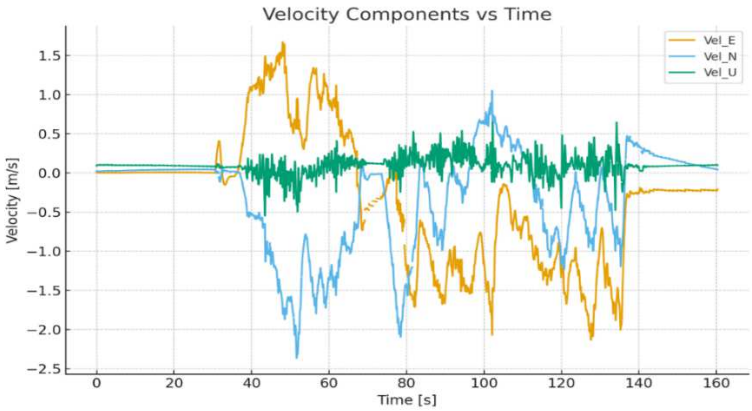

Fig. 13 GNSS velocity components (East, North, Up) over time

The results indicate a maximum speed of approximately 2.5 m/s and a mean velocity of roughly 0.9 m/s in Fig. 14. The irregular profile and frequent speed reductions correspond to transient slip and reduced traction caused by sand deformation beneath the wheels. Simultaneously, acceleration spikes recorded by the IMU (see Fig. 11) confirm the dynamic coupling between the terrain response and robot motion.

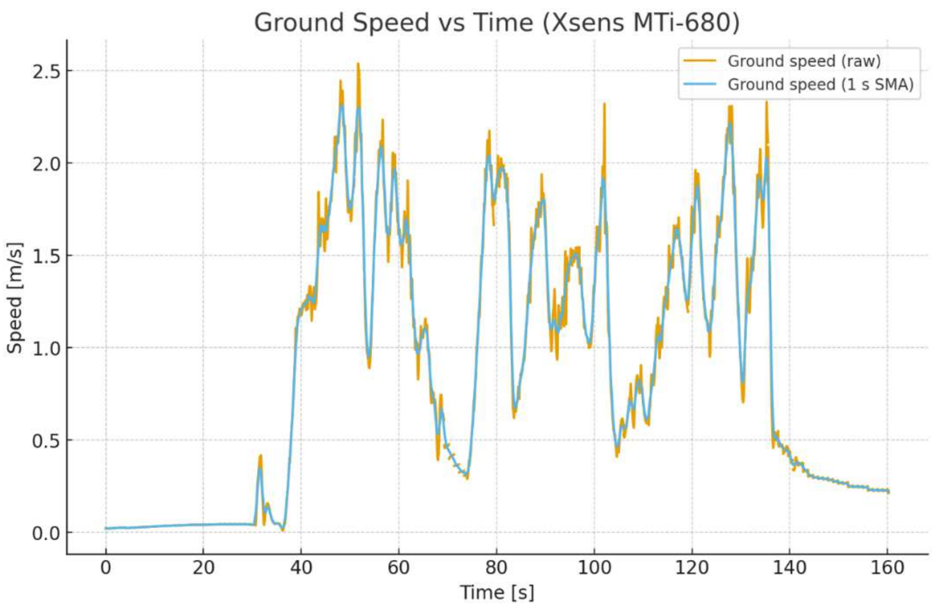

Fig. 14 Ground speed over time computed from GNSS velocity components

The linear speed was additionally calculated and filtered from the IMU acceleration data to evaluate how inertial sensing alone can represent the vehicle's motion on unstructured terrain. The longitudinal acceleration component (Acc_X) was corrected for gravity using the recorded orientation (Roll, Pitch, Yaw) from the Xsens MTi-680, assuming the *X*-axis aligned with the robot's forward direction. A brief stationary period at the beginning of the test (approximately 2 seconds) was used to remove the mean acceleration bias. The corrected signal was subsequently filtered with a 0.5-second moving average to reduce high-frequency vibration effects induced by sand deformation and wheel–ground interaction. Finally, the smoothed acceleration was integrated numerically using the trapezoidal rule to obtain speed:

$$\hat{v}_{\mathrm{IMU}}\left(t\right)=\int_{0}^{t}\left(a_X^{\mathrm{lin}}(\tau)-\overline{a}_{\mathrm{bias}}\right)\mathrm{d}\tau \tag{4}$$

The resulting IMU-calculated and filtered speed, presented in Fig. 15, reproduces the main phases of motion observed in the GNSS-based ground speed, confirming that the inertial measurements captured the vehicle's dynamic behavior. However, a gradual drift in the calculated velocity is evident, attributable to small residual acceleration biases and surface-induced vibrations. This demonstrates the typical limitation of purely inertial speed estimation when external position updates are unavailable.

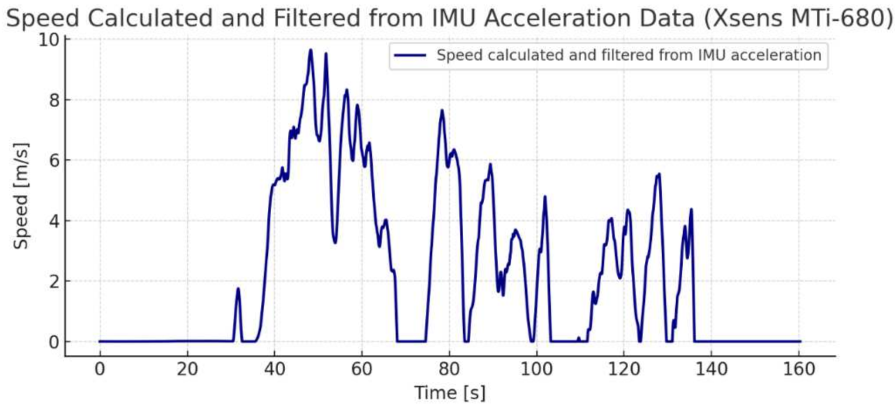

Fig. 15 IMU-based speed estimate after gravity compensation and filtering

For quantitative validation, the ground truth trajectory and velocity extracted from the MTi-680's fused GNSS/INS solution were used as reference data for comparison with the simulated motion generated in the Gazebo environment. The degree of agreement between the measured and simulated speed profiles enables assessment of model fidelity, particularly with respect to wheel-ground interaction and slip characteristics. Despite the overall stability of GNSS reception, small fluctuations in recorded position and velocity demonstrate that even high-quality GNSS signals introduce measurable uncertainty in real-terrain mobility analysis.

The simulation results demonstrate that terrain properties and slope inclination significantly affect both robot mobility and sensor accuracy. On medium-density sand, the robot maintained stable motion with a low slip proxy magnitude, and odometry closely tracked ground-truth velocities, reflecting the surface's high load-bearing capacity. IMU signals exhibited low-amplitude fluctuations, indicating smooth rolling with minimal vibration. GNSS-derived velocities showed limited noise, consistent with reliable performance in well-compacted terrain.

In contrast, motion on loose sand and muddy surfaces revealed substantial discrepancies between commanded and actual velocities. The slip proxy increased, with peaks during acceleration phases of the sinusoidal command. IMU data recorded sharp transients in angular velocity and acceleration, indicating intermittent loss of traction and wheel-surface impacts. Under slope conditions, these effects were amplified – particularly during deceleration – when the gravitational component opposed wheel motion, resulting in temporary immobilization and recovery. GNSS readings exhibited increased jitter during low-speed or stop-and-go motion, indicating reduced reliability of velocity estimates in these regimes.

These results confirm that sensor accuracy is closely tied to traction quality. Odometry errors increase nonlinearly with slip, as wheel rotation no longer represents actual displacement. IMU signals capture the onset of instability but accumulate drift when integrated without external corrections. GNSS maintains overall trajectory consistency but can yield unreliable velocity estimates during vibration or stalling phases, highlighting its sensitivity to dynamic disturbances and intermittent motion.

These findings highlight the need for adaptive multi-sensor fusion guided by terrain classification. Vision-based surface identification can enable the control system to reweight sensor inputs dynamically – for example, relying more on IMU data on stable surfaces, on odometry under moderate traction, and on GNSS corrections when signal integrity is high. Conversely, under deformable or slippery conditions, odometrical data should be down weighted and combined with predictive slip models or learned motion patterns to maintain robust localization.

The limitations of GNSS performance under unstructured conditions – including areas with signal occlusion or reflections, such as forests or industrial sites – further underscore the importance of terrain-aware perception. By classifying surfaces such as sand, mud, or gravel using onboard vision systems (e.g., CNN-based or texture-based classifiers), the robot can adaptively adjust the weighting of odometry, IMU, and GNSS data in real time. This integration of terrain recognition with adaptive sensor fusion provides a foundation for more resilient navigation in unstructured environments, where traction and ground composition vary unpredictably.

The combination of visual terrain identification, slip estimation, and vibration analysis supports the development of intelligent control systems that compensate for wheel skidding, energy losses, and inertial drift. The presented post-processing results and derived physical insights confirm the importance of multi-sensor integration and terrain-adaptive perception for reliable off-road robotic mobility. The proposed analytical framework – based on realistic modeling of terrain physics, slope effects, and sensor uncertainty – constitutes a scalable approach for further research in adaptive motion control, autonomous terrain negotiation, and digital-twin-based prediction of robot behavior on deformable ground.

The findings validate the simulation framework as a digital twin environment capable of replicating the complex physical interactions between the robot and deformable terrain. The combination of realistic surface modeling, slope effects, and sensor-level analysis provides a valuable foundation for developing and testing perception, control, and data fusion algorithms before field deployment.

5 Conclusions and Future Work

This work combined a ROS 2/Gazebo-based digital twin of the Elevate Wheeled Platform with a complementary field sensor study to characterize mobility limitations on deformable, unstructured terrain. The simulation results indicated that cohesive mud can lead to rapid sinkage and vehicle immobilization, whereas loose sand on an inclined surface induces pronounced wheel slip and increased odometry deviations.

Across all evaluated scenarios, wheel odometry exhibited the highest sensitivity to slip, inertial measurements captured short-term dynamic disturbances but suffered from drift when integrated for velocity estimation, and GNSS-derived velocity estimates degraded during low-speed and stop-and-go motion. Future work will focus on calibrating deformable-terrain parameters using controlled experimental data, integrating vision-based terrain classification and online slip estimation to adapt sensor-fusion weighting in real time, and extending validation to a broader set of terrain types and inclination angles.

From a military perspective, the proposed simulation-based evaluation methodology is directly applicable to early-stage assessment and comparative analysis of unmanned ground systems intended for operation in unstructured and degraded environments. By emphasizing observable mobility effects such as traction loss, slip development, and immobilization thresholds rather than predefined mechanical passability limits, the approach aligns with current military research trends that prioritize system-level performance under realistic operational constraints.

In this context, the presented methodology is consistent with ongoing NATO research activities addressing autonomy, mobility, and robustness of ground platforms, including initiatives such as AVT-408, AVT-380, and AVT-435. These efforts underline the importance of repeatable, simulation-supported tools for evaluating vehicle behavior across diverse terrain conditions prior to resource-intensive field trials.

Therefore, the proposed framework can support capability development, concept validation, and risk reduction for military unmanned ground vehicles by enabling systematic analysis of terrain-induced mobility degradation and sensor-based performance limits at an early design stage.

Acknowledgement

The authors would like to thank STEKOP S.A. for providing access to the Elevate Platform to install our sensing equipment and for supporting the real-world field tests. The paper is a part of the research under project 59.24688.PR at the Military Institute of Armored and Automotive Technology in Poland.

References

[1] WANG, N., X. LI, Z. SUO, J. FAN, J. WANG and D. XIE. Traversability Analysis and Path Planning for Autonomous Wheeled Vehicles on Rigid Terrains. *Drones*, 2024, **8**(9), pp. 419-438. DOI 10.3390/drones8090419.

[2] TEJI, M.D., T. ZOU and D.S. ZELEKE. A Survey of Off-Road Mobile Robots: Slippage Estimation, Robot Control, and Sensing Technology. *Journal of Intelligent & Robotic Systems*, 2023, **109**(2), 38. DOI 10.1007/s10846-023-01968-2.

[3] BENRABAH, M., C. OROU MOUSSE, E. RANDRIAMIARINTSOA, R. CHAPUIS and R. AUFRÈRE. A Review on Traversability Risk Assessments for

Autonomous Ground Vehicles: Methods and Metrics. *Sensors*, 2024, **24**(6), 1909. DOI 10.3390/s24061909.

[4] CARVALHO, A., D. PORTUGAL and P. PEIXOTO. On Terrain Traversability Analysis in Unstructured Environments: Recent Advances in Forest Applications. *Intelligent Service Robotics*, 2025, **18**(1), pp. 195-213. DOI 10.1007/s11370-025-00591-4.

[5] KRZYSTAŁA, E., S. SŁAWSKI, T. JAROSZ, A. STOLARCZYK and M. POLIS. Assessment of the Human Threat during the Improvised Explosive Device Detonation. In: *5th Polish Congress of Mechanics, 25th International Conference on Computer Methods in Mechanics*. Gliwice: PCM-CMM, 2023.

[6] DOHNAL, F., Q.T. NGUYEN, M. RYBANSKÝ, V. TALHOFER, M. HUBÁČEK and J. ČAPEK. Automated Determination of Relative Height of Terrain Steps Using a Geoprocessing Model. In: *2023 International Conference on Military Technologies (ICMT)*. Brno: IEEE, 2023. DOI 10.1109/ICMT58149.2023.10171285.

[7] LAURO, O., et al. Terrain Characterization and Classification with a Mobile Robot. *Journal of Field Robotics*, 2006, **23**(2), pp. 103-122. DOI 10.1002/rob.20113.

[8] GUO, J., W. LI, H. GAO, L. DING, T. GUO, B. HUANG and Z. DENG. In-Situ Wheel Sinkage Estimation under High Slip Conditions for Grouser-Wheeled Planetary Rovers: Another Immobility Index. *Mechanism and Machine Theory*, 2021, **158**, 104243. DOI 10.1016/j.mechmachtheory.2021.104243.

[9] GO, S. and G. ISHIGAMI. Modeling of Slip Rate-Dependent Traversability for Path Planning of Wheeled Mobile Robots in Sandy Terrain. *Frontiers in Robotics and AI*, 2024, **11**, 1320261. DOI 10.3389/frobt.2024.1320261.

[10] NOHEL, J., P. STODOLA, Z. FLASAR and M. RYBANSKY. Multiple Maneuver Model of Cooperating Ground Combat Troops. *Journal of Defense Modeling and Simulation*, 2023, **20**(4), pp. 481-493. DOI 10.1177/15485129221078939.

[11] RYBANSKY, M., M. BRENOVA, J. CERMAK, J. VAN GENDEREN and A. SIVERTUN. Vegetation Structure Determination Using LIDAR Data and the forest Growth Parameters. In: *8th IGRSM International Conference and Exhibition on Remote Sensing & GIS*. Kuala Lumpur: IOP Publishing, 2016, **37**, 012031. DOI 10.1088/1755-1315/37/1/012031.

[12] RYBANSKY, M., V. KRATOCHVIL, F. DOHNAL, R. GEROLD, D. KRISTALOVA, P. STODOLA and J. NOHEL. GNSS Signal Quality in Forest Stands for Off-Road Vehicle Navigation. *Applied Sciences*, 2023, **13**(10), 6142. DOI 10.3390/app13106142.

[13] SINGH, M., J. KAPUKOTUWA, E.L.S. GOUVEIA, E. FUENMAYOR, Y. QIAO, N. MURRAY and D. DEVINE. Comparative Study of Digital Twin Developed in Unity and Gazebo. *Electronics*, 2025, **14**(2), 276. DOI 10.3390/electronics14020276.

[14] SINGH, M., J. KAPUKOTUWA, E.L.S. GOUVEIA, E. FUENMAYOR, Y. QIAO, N. MURRY and D. DEVINE. Unity and ROS as a Digital and Communication Layer for Digital Twin Application: Case Study of Robotic Arm in a Smart Manufacturing Cell. *Sensors*, 2024, **24**(1), 5680. DOI 10.3390/s24175680.

[15] LI, J. and S.X. YANG. Digital Twins to Embodied Artificial Intelligence: Review and Perspective. *Intelligent Robotics*, 2025, **5**(1), pp. 202-227. DOI 10.20517/ir.2025.11.

[16] KANG, R., Z. DONG and J. HE. Digital Twin for Mobile Robot Modeling and Simulation. *Journal of Physics: Conference Series*, 2024, **2803**(1), 012060. DOI 10.1088/1742-6596/2803/1/012060.

[17] NISHISHITA, T. and G. ISHIGAMI. Slip Estimation Model for Traversability-Based Motion Planning of Cargo Rover on Extraterrestrial Surface. *Frontiers in Robotics and AI*, 2025, **12**, 1638667. DOI 10.3389/frobt.2025.1638667.

[18] REGINALD, N., O. AL-BURAIKI, T. CHOOPOJCHAROEN, B. FIDAN and E. HASHEMI. Visual–Inertial–Wheel Odometry with Slip Compensation and Dynamic Feature Elimination. *Sensors*, 2025, **25**(5), 1537. DOI 10.3390/s25051537.

[19] HRABAR, I., G. VASILJEVIĆ and Z. KOVAČIĆ. Estimation of the Energy Consumption of an All-Terrain Mobile Manipulator for Operations in Steep Vineyards. *Electronics*, 2022, **11**(2), 217. DOI 10.3390/electronics11020217.

[20] VAGAŠ, M. and J. ROMANČÍK. Calibration of an Intuitive Machine Vision System Based on an External High-Performance Image Processing Unit. In: *24th International Conference on Process Control (PC)*. Štrbské Pleso: IEEE, 2023, pp. 186-191. DOI 10.1109/PC58330.2023.10217606.

[21] BORGES, P., et al. A Survey on Terrain Traversability Analysis for Autonomous Ground Vehicles: Methods, Sensors, and Challenges. *Field Robotics*, 2022, **2**(1), pp. 1567-1627. DOI 10.55417/fr.2022049.

[22] *Unmanned Vehicle* [online]. [viewed 2025-08-10]. Available from: https://stekopsystems.pl/pojazdy-bezzalogowe/elevate/